

POWER-HIL TESTING OF LI-PO BATTERY PACKS FOR LIGHTWEIGHT EVTOL UAVS

Aleksander Suti[1], Marc Budinger[1], Gianpietro Di Rito[2], Aurélien Reysset[1] & Ion Hazyuk[1]

[1]Dep. of Mechanical Engineering, ICA, Université de Toulouse, UPS, INSA, ISAE-SUPAERO, MINES-ALBI, CNRS, ICA,3 rue Caroline Aigle, Toulouse, 31400, France
[2]Dep. of Civil and Industrial Engineering, University of Pisa, 2 Largo Lucio Lazzarino, Pisa, 56126, Italy

Abstract

The performances of UAVs with electric propulsion strongly depend on the efficiency of onboard energy storage systems, which is essentially governed by the Battery Management System (BMS). The design of advanced BMS algorithms, capable of accurate estimation of battery states, play a key role in maximizing flight time and extending battery life for UAV applications. Once developed the estimation algorithms, realistic validation using a battery pack becomes necessary, which can be effectively achieved through Power Hardware-in-the-Loop (P-HIL) testing. This paper proposes a P-HIL framework for the Li-Po battery system of a lightweight eVTOL UAV, in which one (out of 18) of the battery packs is required to deliver the current request derived from a real-time dynamic simulation of the UAV dynamics, while operating within a wind tunnel to realistically replicate the enviromental conditions experienced during flight (temperature, cooling airflow, etc.). The proposed P-HIL setup enables continuous monitoring of the battery pack condition over successive flight missions, thereby allowing validation of the BMS across all battery states throughout its life cycle.

Keywords: Li-Po Battery Pack, Battery Pack Ageing, Power-HIL testing, Electric Propulsion System, eVTOL UAVs

1. Introduction

In the context of airborne vehicle electrification, Unmanned Aerial Vehicles (UAVs) have emerged as effective platforms for prototyping and validating electrification strategies relevant to future manned aviation systems [1], as electrification significantly affects flight performance (e.g., endurance) and system reliability. In particular, flight endurance is predominantly influenced by the onboard energy storage system. Lithium Polymer (Li-Po) batteries currently dominate the market for small UAVs due to their favorable balance between energy density (approximately 100–200 Wh/kg) and power density (around 200–1000 W/kg), which makes them well suited to UAV applications [2, 3, 4, 5].

Battery performance can vary significantly depending on operating conditions and degradation state [4]. For this reason, the energy storage module, typically composed of multiple battery cells connected in series and parallel, is equipped with a Battery Management System (BMS). The primary objective of the BMS is to optimize battery utilization to extend cycle life and flight time while ensuring safe and reliable operation [2]. Among the various battery states, the State of Charge (SOC), State of Temperature (SOT), and State of Health (SOH) play a crucial role in determining lithium battery performance [6, 7, 8]. Consequently, the monitoring function of the BMS must be capable of accurately estimating these states to guarantee operation within safe and optimal limits.

Following a Model-Based Design approach [9], in previous works [10, 11], the authors developed SOC and SOT estimators based on model-based observer algorithms and validated them through Model-in-the-Loop (MIL), Processor-in-the-Loop (PIL), and Hardware-in-the-Loop (HIL) testing. To enable the development of a State of Health (SOH) estimator and to validate the complete state

estimation framework in a more realistic operational environment, a Power Hardware-in-the-Loop (P-HIL) testing [12] framework is developed in this work.
The proposed P-HIL framework is based on a real-time simulation of the reference UAV flight dynamics, including the Flight Control Computer (FCC) and propulsion system models. This simulation generates the reference current demand required by the Battery Pack (BP), while a dedicated power amplifier draws the corresponding current from the physical battery pack under test. The battery pack is installed within a 3D-printed equivalent UAV boom element and operated inside a temperature-controlled wind tunnel to realistically emulate both its physical location within the UAV and in-flight environmental conditions. Battery temperature, ambient temperature, current, and voltage measurements are provided to a microcontroller board used for battery state estimation, as well as to the real-time UAV simulator. This configuration allows the real battery voltage to directly constrain the propulsion system model, thereby reproducing the interaction between available battery voltage and electronic speed controller operation.
This approach enables comprehensive testing of both the reference battery pack and its monitoring system under realistic operating conditions, while also allowing characterization of battery behavior under ageing effects [13, 14]. In this context, the proposed P-HIL framework allows system validation up to Technology Readiness Level (TRL) 5–6 [15], as it enables testing in a relevant environment with representative operational conditions. The study focuses on a 6-cell, 22.2 V, 2000 mAh Li-Po battery pack employed in a 25 kg dual-electric Vertical Take-Off and Landing (eVTOL) UAV.

2. Materials and Methods

2.1 Reference UAV architecture

The reference platform, schematically shown in Figure 1, is a 25 kg eVTOL UAV featuring two groups of non-tilting rotors: eight motors dedicated to vertical take-off, landing, and low-speed maneuvering, and two motors used for forward flight.

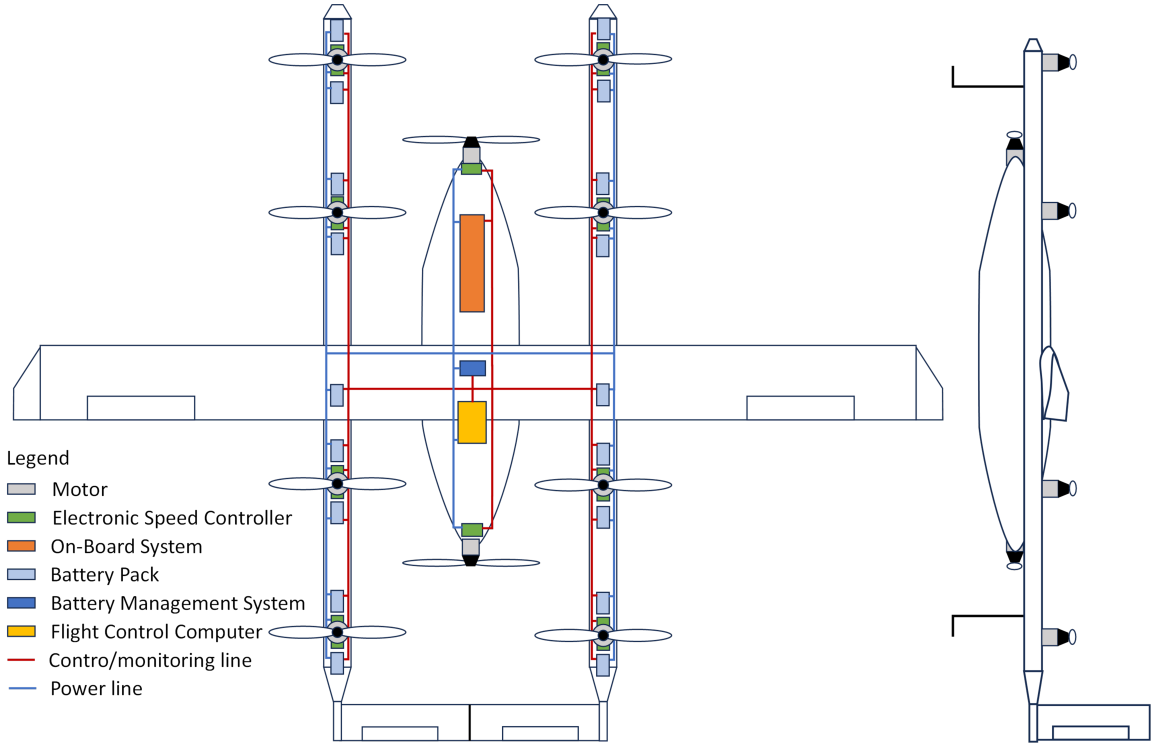


Figure 1 – Conceptual schematic of the reference eVTOL UAV: (left) top view, (right) side view.

The propulsion system employs brushless DC electric motors driving two-blade, fixed-pitch propellers through dedicated Electronic Speed Controllers (ESCs). The onboard energy is provided by a Battery Pack System (BPS) composed of 18 battery packs (2000 mAh, 22.2 V each) directly connected in series; no DC–DC converters are included in this configuration. Additional system components

include onboard systems and payload, with a total power demand of approximately 250 W, a Battery Management System (BMS), and a Flight Control Computer (FCC).

2.2 UAV and power systems modelling

2.2.1 Longitudinal flight dynamics

The power request to the UAV propulsion system can be essentially derived from the simulation of the longitudinal dynamics of the vehicle. Hence, the non-linear longitudinal dynamics of the UAV in the body-axis reference frame is described, with reference to Figure 2, by the following set of equations [16]:

$$\begin{cases} \dfrac{du}{dt} + wq = -g\,sin(\theta) + \dfrac{1}{m_{TO}}(L\,sin(\alpha) - D\,cos(\alpha) + F_{px}) \\ \dfrac{dw}{dt} - uq = g\,cos(\theta) - \dfrac{1}{m_{TO}}(L\,cos(\alpha) - D\,sin(\alpha) + F_{pzf} + F_{pzb}) \\ \dfrac{dq}{dt} = \dfrac{1}{I_{yy}}(M_a + M_b) \\ \dfrac{d\theta}{dt} = q \end{cases} \tag{1}$$

where u, w (F_{px} and F_{pz}) are the linear velocities (propulsion system forces, thrusters and lifters respectively) along the x_B and z_B body axis, respectively, while q and I_{yy} are the angular speed and the moment of inertia along y_B. The mass of the UAV is denoted as m_{TO} and g represents the gravitational acceleration. The aerodynamic loads include L and D lift and the drag forces, while M_a as aerodynamic torque. The torque produced by the propulsion system lifters is M_p, and the angle of attack and the peach angle are represented by α and θ respectively.

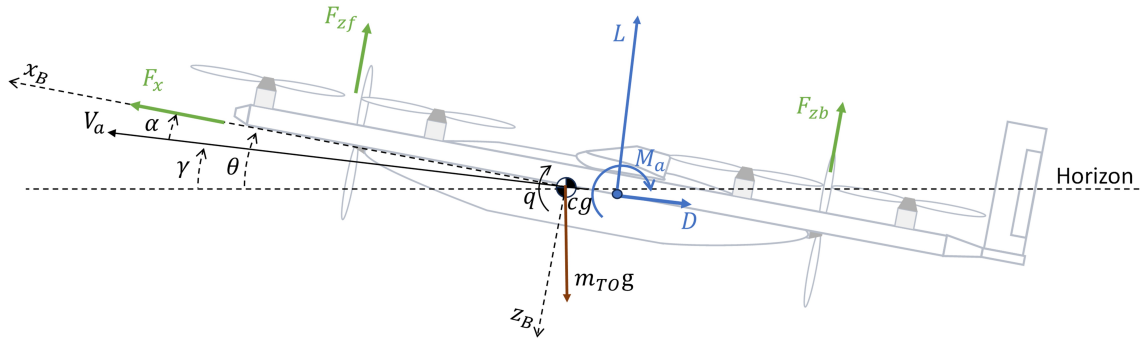


Figure 2 – Longitudinal free-body diagram of the reference UAV.

Adding the navigation equations, a sixth states system with four inputs is obtained.

$$\begin{cases} V_h = u\,cos(\theta) + w\,sin(\theta) \\ V_v = u\,sin(\theta) - w\,cos(\theta) \\ \gamma = \dfrac{V_v}{V_a} \end{cases} \tag{2}$$

where V_h, $V_v$and V_a are the horizontal speed, the vertical speed and the true air speed of the UAV, while γ is the trajectory angle.

2.2.2 Guidance, Navigation and Control

The UAV flight mission control architecture, schematically reported in Figure 3, utilizes a nested-loop structure to manage both trajectory and speed in the longitudinal plane. The inner loop, responsible for controlling the horizontal and vertical velocities, employs a Linear Quadratic Integral (LQI) control strategy[]. This choice of LQI control allows for enhanced handling of the transition phase between copter mode and fixed-wing mode, providing stability and responsiveness as the UAV switches flight

modes. The outer loop, primarily governing altitude, is based on a Proportional-Integral (PI) regulator to ensure altitude tracking and timely correction throughout flight, while the longitudinal position control is activated during VTOL flight phases. For the LQI controller, gains matrix are synthesized from the linearized dynamics of the UAV at varying advance speed trim conditions. Specifically, two primary gain matrices are designed: one for low-speed control (i.e., V_h < 14 m/s) and another for high-speed control. The transition between these control matrices is achieved through interpolation, allowing a smooth shift between low-speed and high-speed dynamics.

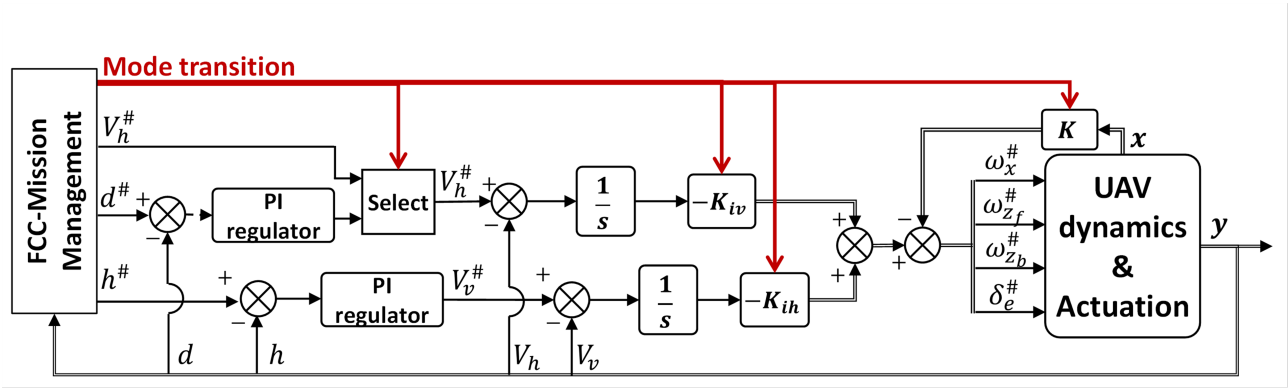


Figure 3 – Working scheme of the closed-loop controls for stability augmentation, guidance and navigation of the UAV.

2.2.3 Propulsion system

The propulsion-system dynamics are modeled with reference to Figure 4(a) through Equation (3), assuming a rigid mechanical transmission between the output shaft and the propeller hub for the aero-mechanical subsystem. The electrical subsystem, comprising the BLDC motor and power electronics, is instead represented by a reduced-order phase-to-phase model based on a six-step converter commutation strategy [16].

$$\begin{cases} J_{\text{em}}^{(eq)}\,\dot{\omega}_{em} = Q_{em} - Q_p \\ Q_p = C_Q(\omega_p, AR)\,\rho\,D_p^5\,\omega_p^2 \\ AR = \dfrac{V_{ap}}{D_p\,\omega_p} \\ Q_{\text{em}} = k_t\,I_{\text{em}} \\ V_{\text{em}} = R_{pp}\,I_{\text{em}} + L_{pp}\,\dot{I}_{\text{em}} + k_v\,\omega_{\text{em}} \end{cases} \tag{3}$$

In Equation (3), $J_{em}^{(eq)}$, Q_{em} and ω_{em} are the shaft equivalent inertia, the electromagnetic and the angular speed of the motor, while Q_p, C_Q, AR and D_p are the resistant torque, the torque coefficient, the advance ratio and the diameter of the propeller, respectively. The mechanical transmission between the propeller and the electric motor output shaft is assumed rigid, hence the propeller angular position ω_p equals the motor's one. The axial wind speed of the propeller is indicated with V_{ap}. For the electrical section V_{em}, I_{em}, R_{pp} and L_{pp} are the phase to phase voltage, current, resistance and inductance, respectively. The motor speed, and torque constant are indicated with k_v and k_t, respectively. For the closed-loop control of the electric motor, two nested control loops are considered, acting respectively on propeller speed and motor current. All regulators implement proportional–integral control actions based on the corresponding tracking errors. To mitigate the effects of actuator saturation, each control loop is equipped with an anti-windup mechanism based on a back-calculation algorithm.

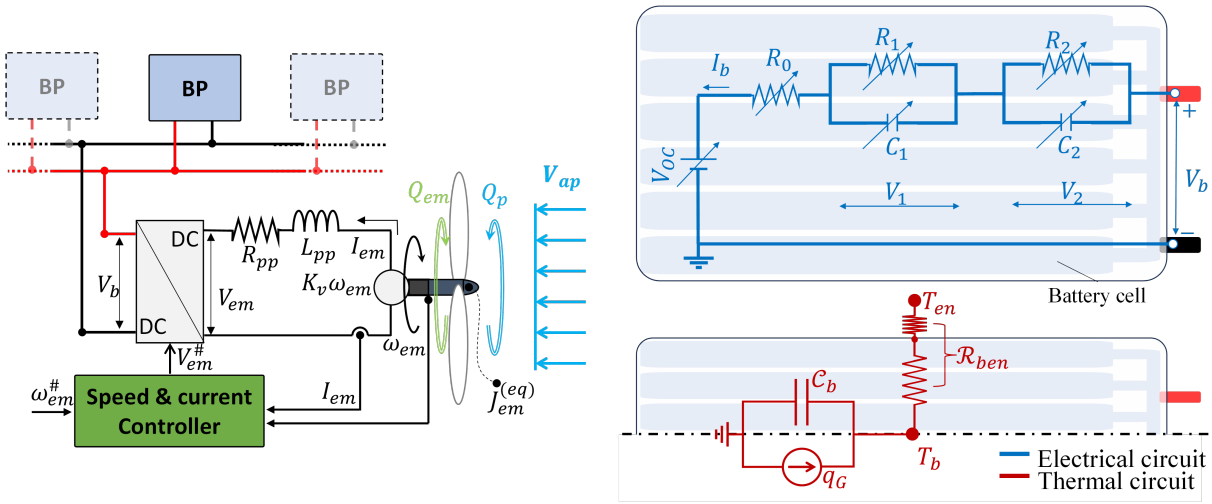


Figure 4 – Scheme of the propulsion system modelling. (left) focus on the electric drive; (right) focus on the of battery pack.

2.2.4 Battery pack system

The energy storage system of the reference platform is mainly composed of a set of Li-Po battery packs connected in parallel to increase flight endurance, together with a Battery Management System (BMS) for state monitoring. In this work, a battery pack is modeled using an electro-thermal equivalent circuit, as schematically shown in Figure 4 (b), [17, 18], via the following:

$$\begin{cases} \dfrac{dSOC}{dt} = \dfrac{I_b}{Q_{b0}} \\ \dfrac{dV_1}{dt} = \dfrac{I_b}{C_1(SOC,T_b)} - \dfrac{V_1}{R_1(SOC,T_b)\cdot C_1(SOC,T_b)} \\ \dfrac{dV_2}{dt} = \dfrac{I_b}{C_2(SOC,T_b)} - \dfrac{V_2}{R_2(SOC,T_b)\cdot C_2(SOC,T_b)} \\ \dfrac{dT_b}{dt} = \dfrac{q_G}{C_b} - \dfrac{T_b - T_{en}}{C_b R_{ben}} \\ q_G = \left[V_b - V_{OC}(SOC,T_b) + T_b\dfrac{\partial V_{OC}}{\partial T_b}\right] I_b \\ \dfrac{\partial V_{OC}}{\partial T_b} = f(SOC,T_b) \\ V_b = V_{OC}(SOC,T_b) + R_0(SOC,T_b)I_b + V_1 + V_2 \end{cases} \tag{4}$$

With reference to the electrical dynamics, V_b and V_{OC} are the terminal model output voltage and the Open Circuit Voltage (OCV), while R_0 denotes the internal resistance. The two RC-grid are characterized by the voltage drops V_1 and V_2, the capacitances C_1, and C_2, and by the resistances R_1, and R_2, while the battery total capacity is denoted by Q_{b0}. The heat source q_G accounts for both overpotential heat ($I_b(V_{OC} - V_b)$), and by the entropic one ($I_b\left(\dfrac{\partial V_{OC}}{\partial T_b}\right)$), [19]. With reference to the thermal dynamics the battery C_b, and R_{ben} represent the equivalent thermal capacity and the equivalent thermal resistance between the core temperature T_b and the coolant medium, which is in this case the same as the ambient temperature T_{en}.

2.3 Battery Pack model identification testing

To identify the parameters of the reference battery pack model, a Hybrid Pulse Power Characterization (HPPC) test campaign was carried out in previous work by the authors [11]. The HPPC test facilitates the parameter identification process as a function of the battery state of charge (SOC), since the battery is subjected to pulse-current charge and discharge cycles of constant amplitude and duration (test input I_b), while the terminal voltage (test output V_b) is measured. This procedure

enables the identification of the model parameters at different SOC levels. Additionally, by repeating the HPPC test under controlled temperature conditions, it is possible to evaluate the influence of temperature on the battery parameters. In the reference characterization, pulse currents with a duration of 30 min and an amplitude of 5.5 A as shown in Figure 5 (corresponding to the rms value of current along a flight mission of the reference UAV) were applied under controlled environmental conditions representative of hot ($50\,^{\circ}\mathrm{C}$), ambient ($15\,^{\circ}\mathrm{C}$), and cold ($0\,^{\circ}\mathrm{C}$) operating scenarios.

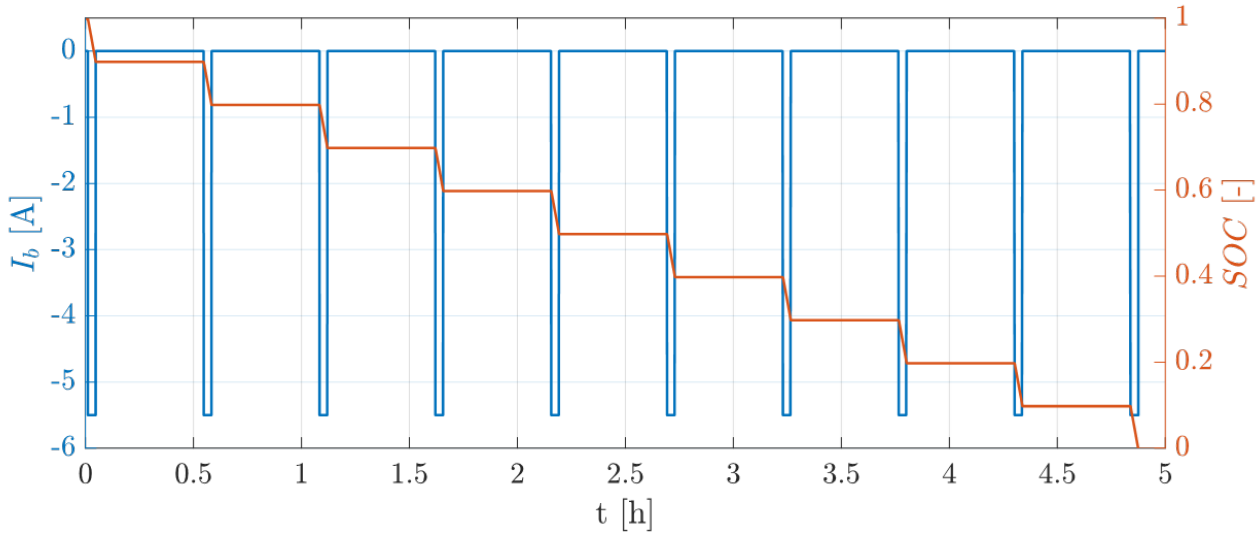


Figure 5 – Reference HPPC test current input.

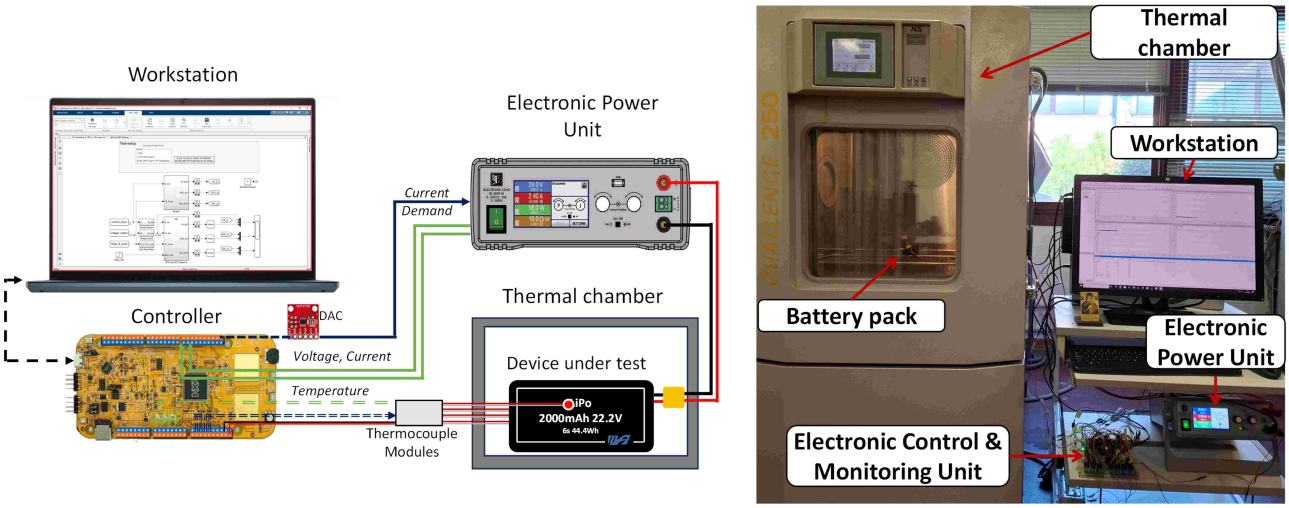


Figure 6 – Battery pack test bench setup at DICI-University of Pisa Fly-By-Wire Laboratory: (left) Functional diagram of the experimental set-up. (right) experimental set-up.

The functional diagram and test equipment of the experimental setup used for the HPPC campaign are shown in Figure 6. The test logic, monitoring algorithms, and protection functions were developed in MATLAB/Simulink and deployed on an NXP S32K144EVB microcontroller. The microcontroller interfaces with an electronic load simulator (Electronic Power Unit EA-EL 9000 DT, 500 W), which applies the current load to the battery and provides voltage and current feedback. The NXP board also manages the acquisition of temperature measurements from thermocouples interfaced with MAX6675 modules for temperature sensing.

2.4 Battery pack Power-HIL test set-up

Power Hardware-in-the-Loop (P-HIL) simulations facilitate the evaluation of power, control, and monitoring systems at nominal power levels. By utilizing actual voltages and currents, these simulations

allow for rigorous validation of components, such as battery packs and inverters, under emulated real-world conditions. The reference P-HIL, which is primarly developed to test battery packs and their BMS, are shown in Figures 7 in terms of functional diagram and the corresponding experimental setup . The test management and high-level control logic are implemented on a workstation (WS), which interfaces with a real-time machine (RTM) based on the Speedgoat Performance platform [20]. The RTM is equipped with an IO131 module with 16-bit analog input and output signals and an IO171 module for the acquisition of ungrounded thermocouples.

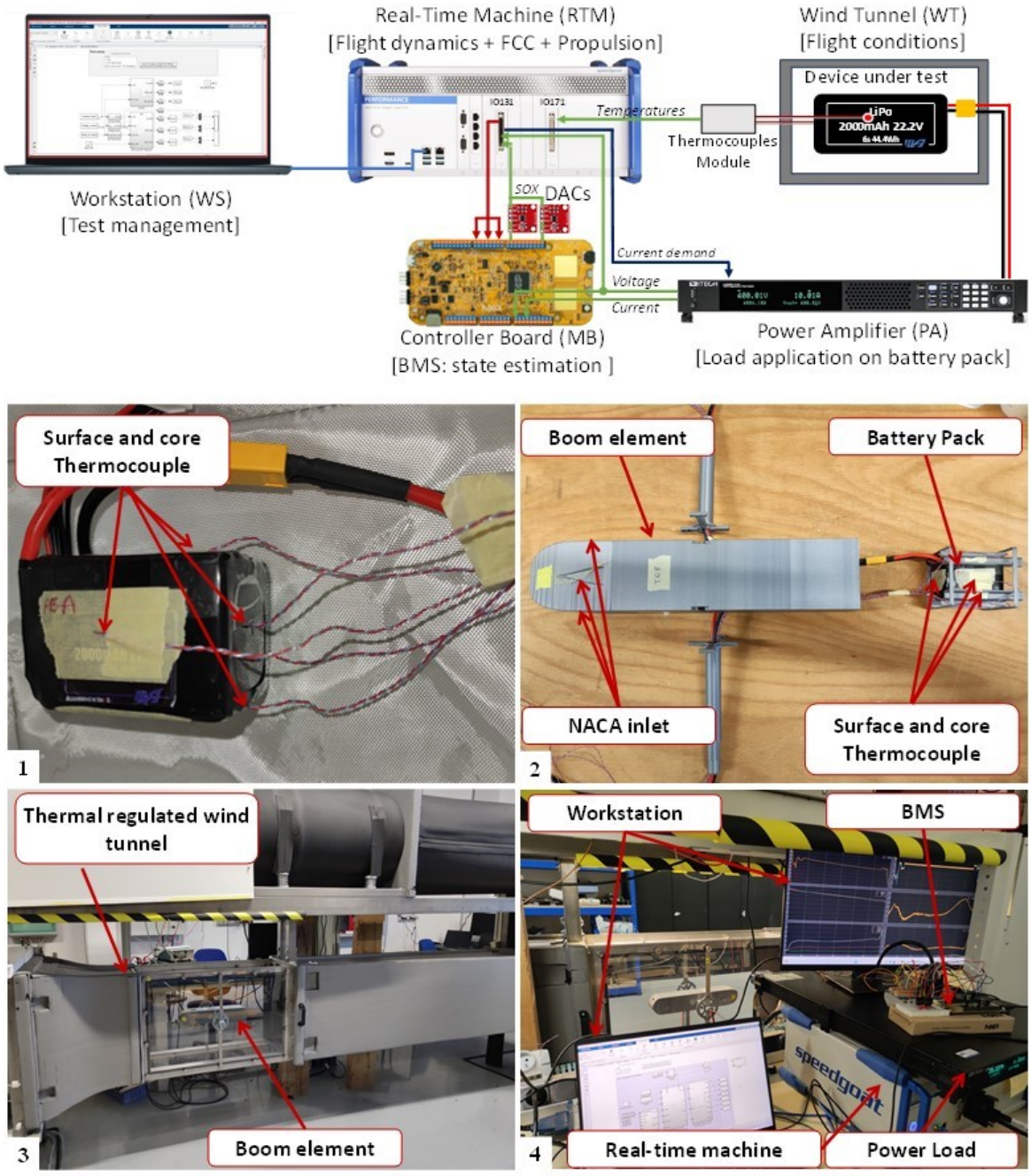


Figure 7 – BP P-HIL testing at Clément Ader Institute(ICA) Laboratory, INSA-Toulouse: (top) Functional diagram; (bottom) Experimental set-up highlighting: Battery pack equipped with termocopules (1); boom element for battery pack housing (2); wind tunnel equipped with the boom element (3); workstation, real-time machine, power load and BMS (4).

The RTM executes the real-time simulation of the reference UAV flight dynamics together with the FCC and propulsion system models. The simulation is driven by the requested UAV speed and altitude trajectory, as shown in Figure 8(a) where is illustrates the altitude over time, as well as

the different flight phases, distinguishing between the two flight modes: Forward (FW) mode and VTOL mode. In addition to the altitude trajectory, the figure also reports the corresponding Rate of Climb (RoC) and Rate of Descent (RoD), providing further insight into the dynamic power demands encountered during each phase of flight. The flight simulator generates, in real-time, the reference current demand required for a single BP, an example is shown in Figure 8(b). The resulting current command is then processed by a power amplifier (PA), which draws the corresponding current from the physical battery pack under test. The BP is installed within a 3D printed UAV boom element and operated in a temperature-controlled wind tunnel to emulate real flight conditions in different scenarios.

Battery pack temperature and ambient temperature are measured using thermocouples interfaced with the RTM via the IO171 module. Battery current and voltage, measured directly by the PA, are provided both to an NXP S32K144EVB microcontroller board (MB) [21], used as BMS for battery state estimation (e.g., SOC, State of Temperature, State of Health), and to the RTM. The The latter uses these signals to interact with the electronic speed controller model of the propulsion system by enforcing voltage limitations, thereby constraining the maximum allowable propeller speed during the simulated flight mission. More about the reference BMS and state estimation can be found in a previous work from the authors [11].

Finally, P-HIL testing is managed and programmed within the MATLAB/Simulink environment. This framework enables deployment of the plant and system models on the Speedgoat target machine, configuration of the RTM I/O interfaces, and communication with the BMS. It also allows the implementation and execution of battery monitoring and estimation algorithms on the microcontroller through its I/O ports.

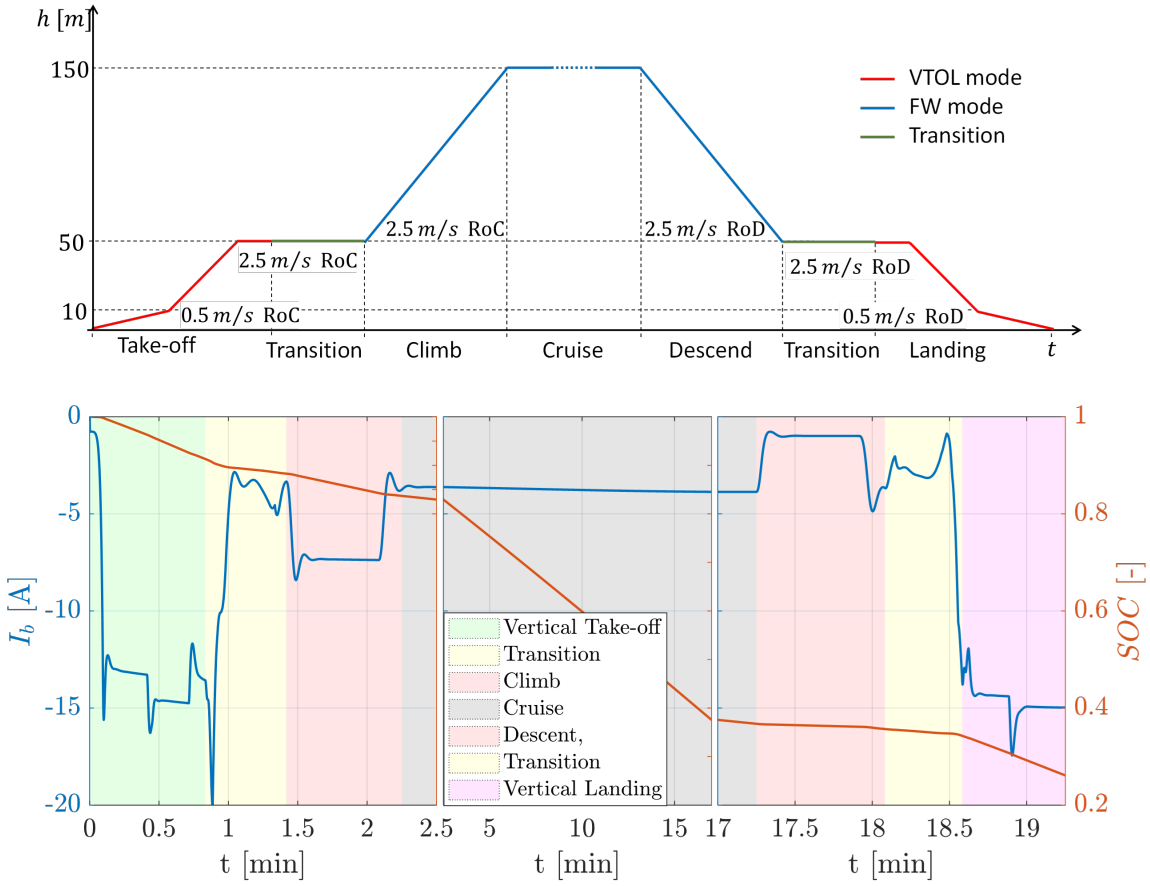


Figure 8 – Flight mission profile : (top) UAV required altitude as function of time; (bottom) simulated reference current profile over time scaled to a single battery pack.

3. Results and Discussion

3.1 Model Validation

An excerpt of the model validation results obtained from the experimental campaign is shown in Figure 9, where the experimental measurements are compared with the response of the identified electro-thermal model. The voltage error remains below 1 V for SOC levels above 10%, while the core temperature error consistently remains below 0.5 ℃. In this case, the State of Charge (SOC) is estimated using the coulomb counting technique. The HPPC test was designed to identify model parameters at discrete SOC intervals of 10%. This level of discretization may partially explain the higher errors observed at lower SOC levels, where the battery parameters tend to exhibit steeper gradients and stronger nonlinear behavior. As a result, even small deviations in the parameter-SOC relationship can lead to larger estimation errors in this operating region. Nevertheless, the overall error remains limited, and the SOC estimation can still be considered reliable across the full operating range..

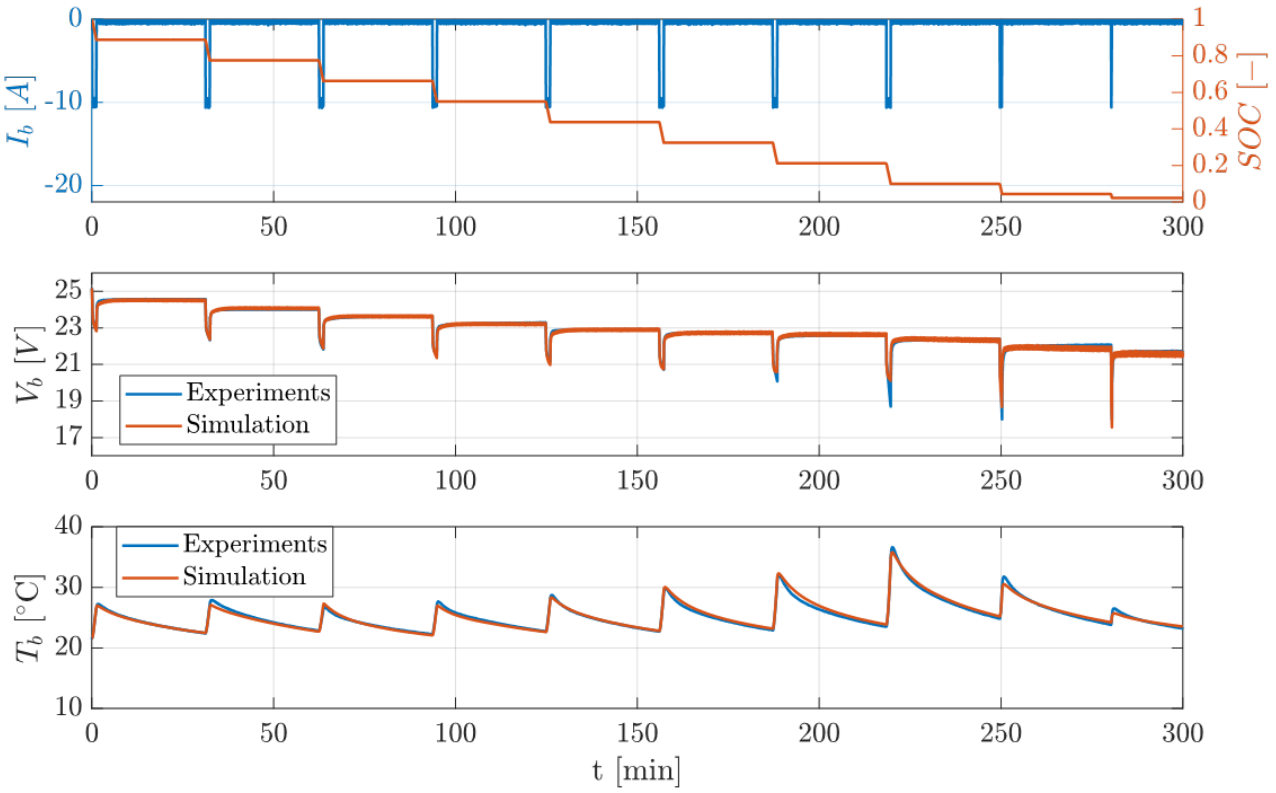


Figure 9 – Battery model results and experimental data comparison with HPPC tests : (top) current input and SOC Coulomb counting; (middle) terminal voltage; (bottom): core temperature.

3.2 BP Power-HIL test

The results of the Power-HIL test related to the UAV flight dynamics simulation, are proposed in Figure 10 and Figure 11, in terms position and speed along horizontal and vertical direction. From Figure 10(top) can be noticed that the transition manoeuvre from VTOL mode to forward flight is performed at a constant altitude of 50 m due to safety reasons. while an interesting aspect observed in the horizontal speed profile (Figure 11(top)) is the smooth variation from 0 to cruise speed, which results from the optimisation process that minimizes the total power required during the transition manoeuvre. During cruise, the horizontal speed is regulated at 22 m/s, which corresponds to the UAV's maximum efficiency speed, while the rate of climb and descent is set to 2.5 m/s, as shown in Figure 11. Under these conditions, the achieved horizontal range is approximately 22 km. The results of the Power-HIL test concerning the propulsion system electric drive are presented in Figure 12, in terms of required power and angular speed for both the thruster drives and the lifter system, scaled

to a single unit. The figures highlight that each thruster exhibits a maximum power of approximately 1 kW at the beginning of the climb phase. The results also show the redistribution of power between the thrusters and the lifter system during the transition phase between VTOL mode and forward flight mode. Finally, the results of a the Power-HIL test concerning the battery system are presented in Figure 13. The test also highlights the performance of the developed State of Charge (SOC) and core temperature estimators, based on Luenberger observers designed by the authors in a previous work [11].

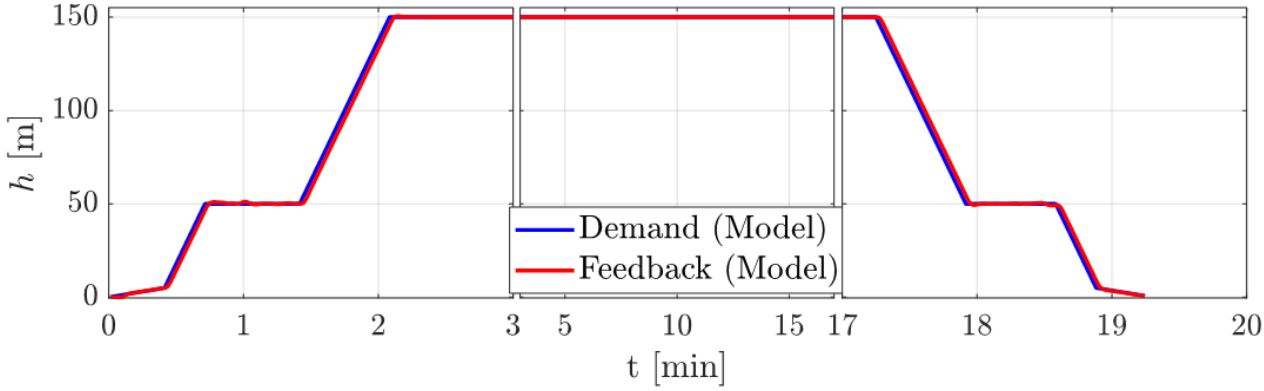


Figure 10 – P-HIL test results for the UAV motion dynamics: (top) altitude; (bottom) horizonal distance.

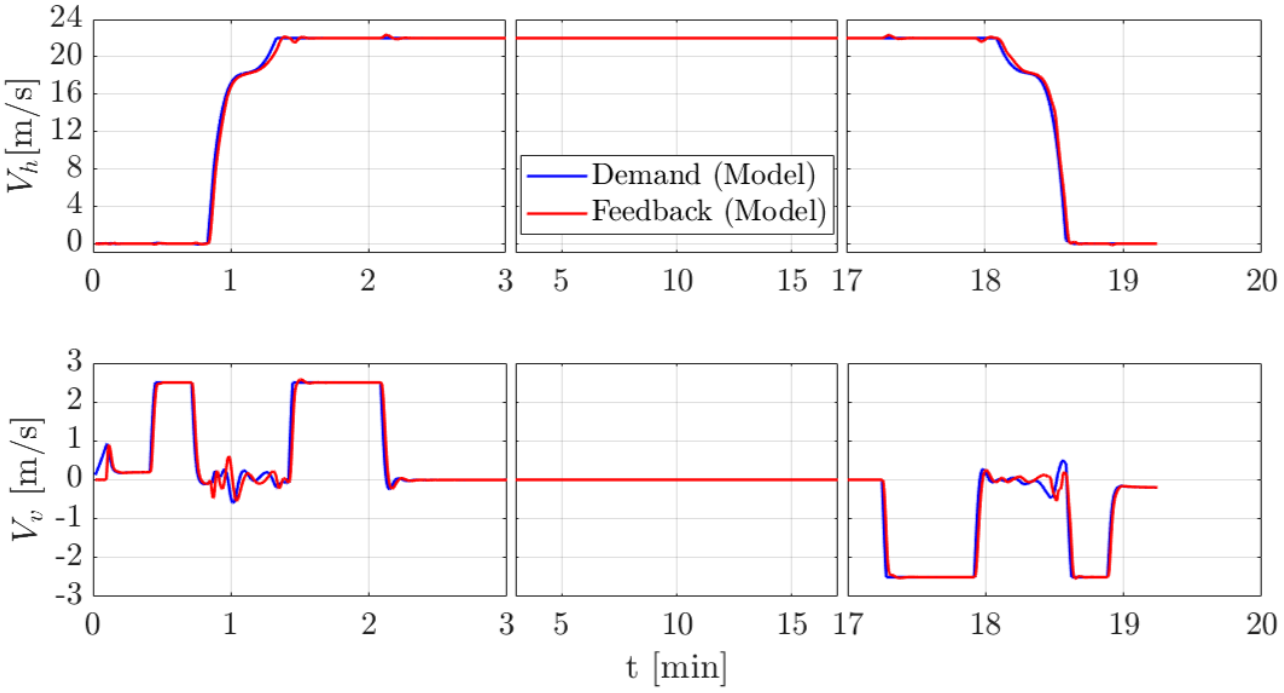


Figure 11 – P-HIL test results for the UAV motion dynamics: (top) horizontal speed; (bottom) vertical speed.

The SOC estimation error increases at low SOC values, reaching a maximum deviation of less than 5%. The estimated core temperature error (Figure 13, bottom) shows a small bias of approximately 2 ℃. The increased error observed in both SOC and core temperature estimation, compared with the model validation results, may be explained by ageing effects caused by the repeated high discharge rates experienced by the battery pack during the flight missions considered in the test campaign. Since the coulomb counting method assumes the Beginning-of-Life (BoL) nominal battery capacity, its accuracy naturally decreases as the battery ages. Similar considerations apply to the temperature estimation error, as battery ageing also affects the thermal response of the system.

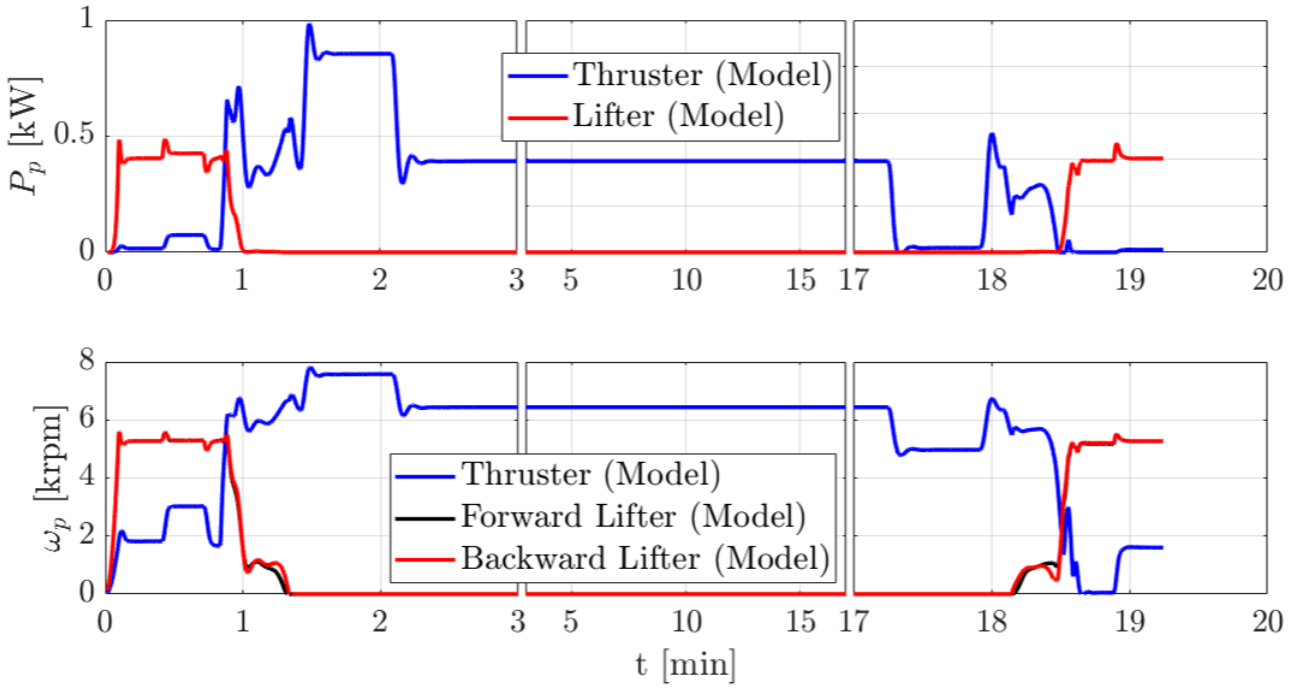


Figure 12 – P-HIL test results for the electric motors and propellers: (top) power of a single thruster and lifter; (bottom) angular speed of a single thruster and lifter.

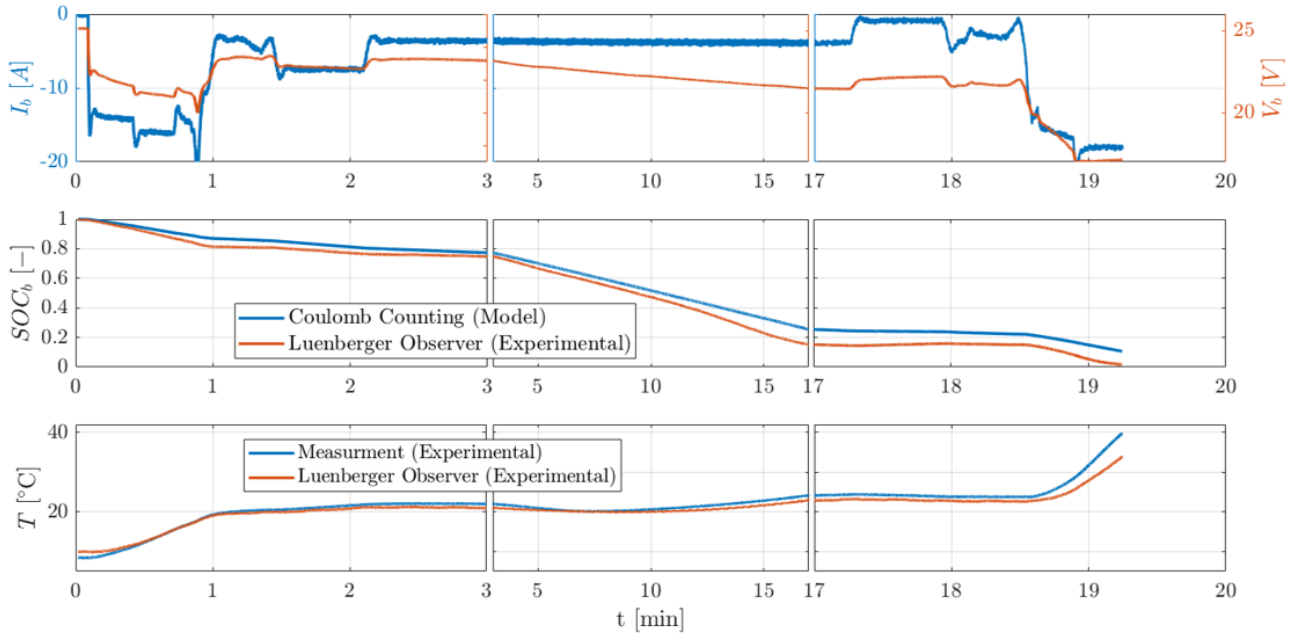


Figure 13 – P-HIL test results of the battery pack (BP): (top) measured current and voltage profiles; (middle) State of Charge estimated using the Coulomb counting method and the Luenberger observer; (bottom) measured core temperature and estimated through Luenberger observer.

The results indicate that the ageing effect on SOC is partially captured by the proposed estimation approach, as the estimated SOC is lower than the value obtained through coulomb counting and reaches zero near the cutoff voltage. However, as ageing progresses and begins to significantly affect the OCV characteristics, the integration of a State of Health (SoH) estimation module becomes essential to ensure accurate and reliable SOC and core temperature monitoring throughout the entire battery lifetime.

4. Conclusions

This work presents activities carried out for the development of a Power Hardware-in-the-Loop (P-HIL) setup for the testing and validation of battery packs and Battery Management Systems (BMS) for lightweight fixed-wing eVTOL UAVs, with the objective of enabling improved performance management, enhanced reliability, and optimized mission planning. The developed P-HIL framework enables system-level testing of propulsion and energy storage components up to Technology Readiness Level (TRL) 5–6, bridging the gap between simulation and relevant operational environments.

To support this objective, an initial modelling campaign was conducted to develop a simplified real-time executable flight simulator of a reference UAV, including the longitudinal motion dynamics and a simplified simulation of the guidance, navigation and flight control system. The flight simulator was then integrated with reduced-order lumped-parameter models of key propulsion system components, including the electric motors, the propellers, and the battery pack, in order to estimate the current demand experienced by each battery pack during a conventional mission profile.

For the battery pack, an experimental campaign was carried out to identify model parameters and characterize its performance through Hybrid Pulse Power Characterization (HPPC) tests conducted at different temperatures. The validated battery model was then used by the authors for the design of model-based state observers for online battery monitoring, as documented in previous work. Subsequently, P-HIL tests were performed using real-time flight mission load profiles to evaluate both the battery pack performance and the effectiveness of the developed state estimation algorithms. To emulate real flight conditions in different scenarios, the BP is installed within a 3D printed UAV boom element and operated in a temperature-controlled wind tunnel.

The developed P-HIL framework also enables the analysis of battery ageing over repeated flight missions. This capability will support future developments of ageing-aware battery models and, consequently, the investigation of the feasibility and limitations of designing estimators for in-flight State of Health (SOH) estimation.

5. Contact Author Email Address

Mailto: suti@insa-toulouse.fr

6. Copyright Statement

The authors confirm that they, and/or their company or organization, hold copyright on all of the original material included in this paper. The authors also confirm that they have obtained permission, from the copyright holder of any third party material included in this paper, to publish it as part of their paper. The authors confirm that they give permission, or have obtained permission from the copyright holder of this paper, for the publication and distribution of this paper as part of the ICAS proceedings or as individual off-prints from the proceedings.

References

[1] Gesang Nugroho, Yoshua Dwiyanson Hutagaol, and Galih Zuliardiansyah. Aerodynamic performance analysis of vtol arm configurations of a vtol plane uav using a computational fluid dynamics simulation. *Drones*, 6:392, 12 2022.

[2] Shiqin Jiao, Guiyang Zhang, Mei Zhou, and Guoqi Li. A comprehensive review of research hotspots on battery management systems for uavs. *IEEE Access*, 11:84636–84650, 2023.

[3] Mohamed Nadir Boukoberine, Zhibin Zhou, and Mohamed Benbouzid. A critical review on unmanned aerial vehicles power supply and energy management: Solutions, strategies, and prospects. *Applied Energy*, 255:113823, 12 2019.

[4] A.G. Olabi, Hussein M. Maghrabie, Ohood Hameed Kadhim Adhari, Enas Taha Sayed, Bashria A.A. Yousef, Tareq Salameh, Mohammed Kamil, and Mohammad Ali Abdelkareem. Battery thermal management systems: Recent progress and challenges. *International Journal of Thermofluids*, 15:100171, 8 2022.

[5] Gianpietro Di Rito, Aleksander Suti, Andrea Ricci, Roberto Galatolo, and Giuseppe Mattei. Experimental characterisation of li-po battery packs and bldc machines for hybrid propulsion systems of lightweight uavs. In *2022 IEEE 9th International Workshop on Metrology for AeroSpace (MetroAeroSpace)*, pages 49–53. IEEE, 6 2022.

[6] Young Woo Son, Deokhun Kang, and Jonghoon Kim. Passive battery thermal management system for an unmanned aerial vehicle using a tetrahedral lattice porous plate. *Applied Thermal Engineering*, 225:120186, 5 2023.

[7] Q.L. Yue, C.X. He, M.C. Wu, and T.S. Zhao. Advances in thermal management systems for next-generation power batteries. *International Journal of Heat and Mass Transfer*, 181:121853, 12 2021.

[8] Foo Shen Hwang, Thomas Confrey, Colin Reidy, Dorel Picovici, Dean Callaghan, David Culliton, and Cathal Nolan. Review of battery thermal management systems in electric vehicles. *Renewable and Sustainable Energy Reviews*, 192:114171, 3 2024.

[9] G. Nicolescu and P. J. Mosterman. *Model-Based Design for Embedded Systems*. CRC Press, 1s edition, 2009.

[10] Aleksander Suti, Gianpietro Di Rito, Marc Budinger, Aurelien Reysset, Ion Hazyuk, and Roberto Di Rienzo. Preliminary design and pil testing of a battery monitoring system for evtol uavs based on an extended kalman filter and electro-thermal model. In *2025 IEEE 12th International Workshop on Metrology for AeroSpace (MetroAeroSpace)*, pages 18–22. IEEE, 6 2025.

[11] Aleksander Suti, Marc Budinger, Gianpietro Di Rito, and Aurélien Reysset. Development and hil validation of observer-based monitoring algorithms of battery packs for evtol uav applications. *Applied Energy*, 401:126637, 12 2025.

[12] MathWorks. Hardware-in-the-loop (hil). Accessed: 2026-01-07.

[13] Simone Barcellona, Morris Brenna, Federica Foiadelli, Michela Longo, and Luigi Piegari. Analysis of ageing effect on li-polymer batteries. *The Scientific World Journal*, 2015, 1 2015.

[14] Daniela Chrenko, Manuel Fernandez Montejano, Sudnya Vaidya, and Romain Tabusse. Aging study of in-use lithium-ion battery packs to predict end of life using black box model. *Applied Sciences*, 12:6557, 6 2022.

[15] Catherine G. Manning. Technology readiness levels, 9 2023.

[16] Aleksander Suti, Gianpietro Di Rito, and Giuseppe Mattei. Hybrid electric propulsion system retrofit for a ice-powered fixed-wing uav via model-based design. *Aerospace Science and Technology*, 176:112158, 9 2026.

[17] Aleksander Suti, Gianpietro Di Rito, and Giuseppe Mattei. Development and experimental validation of novel thevenin-based hysteretic models for li-po battery packs employed in fixed-wing uavs. *Energies*, 15:9249, 12 2022.

[18] Aleksander Suti, Gianpietro Di Rito, and Giuseppe Mattei. Heuristic estimation of temperature-dependant model parameters of li-po batteries for uav applications. pages 269–274. IEEE, 6 2023.

[19] D. Bernardi, E. Pawlikowski, and J. Newman. A general energy balance for battery systems. *Journal of The Electrochemical Society*, 132:5–12, 1 1985.

[20] Speedgoat. Performance real-time target machine. Accessed: 2025-11-14.

[21] NXP. S32k144-q100 evaluation board for automotive general purpose. Accessed: 2025-11-14.